1

Graphite as an Anode Material in Sodium-Ion Batteries

Gustav Åvall[1#], Mustafa Goktas[1#], and Philipp Adelhelm[1,2]

[1] Institute of Chemistry, Humboldt University of Berlin, Berlin Germany
[2] Joint Research Group on Operando Battery Analysis (CE-GOBA), Helmholtz-Zentrum Berlin für Materialien und Energie (HZB), Berlin Germany

COPYRIGHTED MATERIAL

1.1 Introduction

Graphite shows unique abilities as a "storage compound." Its weakly bound layered structure combined with delocalized electrons offers a large chemical variety of intercalation reactions, maybe the most intriguing of which, compared to all other electrode materials used in lithium-ion batteries (LIBs), is the fact that graphite is able to store cations and anions [1]. Today, graphite is by far the most used material for the negative electrode material in LIBs. Natural graphite as well as synthetic graphite are being used. At first sight, the use of graphite in sodium-ion batteries (SIBs) would be only logical. However, among the alkali metals, sodium is the only one showing no appreciable intercalation into graphite. Other approaches are therefore required to use graphite in SIBs.

This chapter will briefly summarize the different types of graphite intercalation compounds (GICs) followed by a discussion on the use of graphite in LIBs and SIBs. Reasons for the limited storage capacity are discussed, followed by a strategy to circumvent this problem. The latter aspect addresses so-called ternary graphite intercalation compounds (*t*-GICs) in which solvent molecules co-intercalate into the graphite lattice along with sodium ions. While *t*-GICs have been known since decades, it was only recently discovered that their formation in electrochemical cells can be highly reversible and very fast. Fundamental aspects of this reaction type are discussed providing an overview of research results that have been obtained in the past years. The chapter concludes with a future outlook on the use of graphite in SIBs.

# Both authors contributed equally.

Sodium-Ion Batteries: Materials, Characterization, and Technology, First Edition.
Edited by Maria-Magdalena Titirici, Philipp Adelhelm, and Yong-Sheng Hu.
© 2023 WILEY-VCH GmbH. Published 2023 by WILEY-VCH GmbH.

1.2 Graphite and Graphite Intercalation Compounds (GICs)

Among the different carbon allotropes (graphite and diamond) and related nanostructures (graphene, nanotubes and nanofibers, and fullerenes), graphite is technologically the most important one. Graphite is composed of planar graphene layers that are stacked with an ABAB stacking sequence, as shown in Figure 1.1, along the *c*-axis (hexagonal graphite). Rhombohedral graphite with ABCABC stacking, as shown in Figure 1.1, exists as well but the structure is thermodynamically less favorable. The bonds within the layers are strongly covalent, whereas weak van der Waals bonds (π–π interactions) exist between the layers [2]. This weak interaction is an important property that allows graphite to act as a host for various molecules and ions, this way forming the family of GICs [2a, 3]. The oldest reports on GICs date back to mid-nineteenth century [4, 5]. These GICs consisted of graphite intercalated by HSO_4^- and H_2SO_4 molecules.

An important characteristic of GIC formation is that the layered structure of graphite remains intact at all times. However, depending on the nature of the stored substance (intercalate), the interlayer spacing as well as the stacking sequence change. Another characteristic is that the intercalation does not occur randomly. Instead, the intercalants tend to order, this way forming periodic structures. With increasing concentration of the intercalate, all interlayer space is eventually filled. The subsequent filling of the graphite is called "staging" and has been observed in the 1930s by Rüdorff and Hofmann [6]. The stage *n* of a GIC formally corresponds to the number of graphene layers between two intercalant layers. For example, stages from $n = 4$ (LiC_{36}) to 1 (LiC_6) have been frequently reported for lithium intercalation into graphite [7]. However, the transition between the different stages is nontrivial, as the intercalants cannot pass through the graphene layers. A peculiar mechanism is therefore required. The commonly accepted model is the domain model suggested by Daumas and Herold in 1969 [8], which is still studied in view of

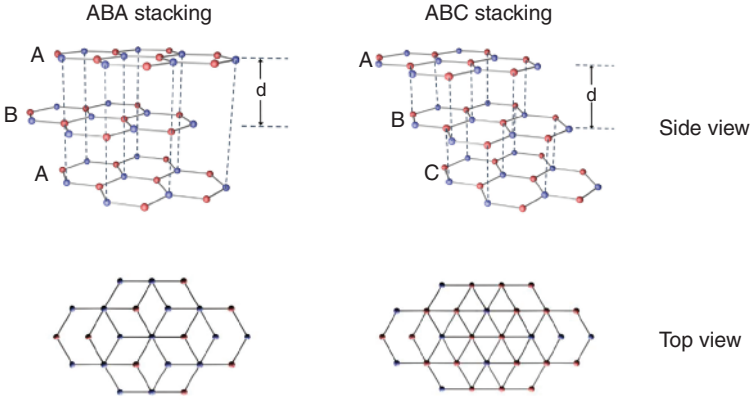

Figure 1.1 (left) The ABA and (right) ABCABC stacking sequence of graphite; *d* indicates the interlayer distance.

kinetics and thermodynamics, especially for Li^+ intercalation [9]. It is worth noting that the type of graphite also can have an influence on the stage transformation as shown for HSO_4^- intercalation, for example [10]. It is clear that intercalation of ions (along with reduction/oxidation of the graphite) will lead to changes in the electrical, magnetic, and thermal properties of the GIC [11]. For example, the color and conductivity of Li-GICs change depending on the stage. A more detailed description on the structure and properties of GICs can be found in a well-known review by Dresselhaus and Dresselhaus [11b] and in the book from Zabel and Solin [12]. In fact, many GICs were intensively studied already in the 1970s and 1980s but thanks to better analytical tools and theory, there is renewed interest in these materials, especially with respect to batteries. This goes beyond Li, Na, or K batteries [13] but also addresses Mg as well as Al batteries [14] or dual-ion batteries (DIBs) [1f, 15].

As mentioned earlier, the family of GICs is very large as many different intercalants exist. For the intercalation of ionic species, the graphite must be either reduced or oxidized to maintain charge neutrality. For example, Li ions intercalate along with reduction of graphite, i.e. formally Li ($Li^+ + e^-$) is added to graphite to form LiC_6 (stage I). In order to classify different GICs, intercalation of cations leads to so-called "donor-type" GICs, whereas intercalation of anions leads to "acceptor-type" GICs. Another way to classify GICs is according to the number of intercalants. Most of the reported GICs are "binary" GICs (*b*-GICs) as they consist of graphite and one type of intercalant. However, also "ternary" GICs (*t*-GICs) or even more complex GICs are reported in which two intercalants intercalate at the same time. This can be, for example, cations and solvent molecules, e.g. such as the here discussed intercalation of Na^+ along with ether solvent molecules to form a $Na(diglyme)_yC_{\sim 20}$*t*-GIC. But also two metals such as Au and K can form *t*-GICs [16]. Other popular examples are halides such as $FeCl_3$ [17], $MoCl_5$ [18], or $AlCl_4^-$, which are nowadays also studied as electrode materials. *t*-GICs can be further classified into homogeneous and heterogeneous ones, depending on how

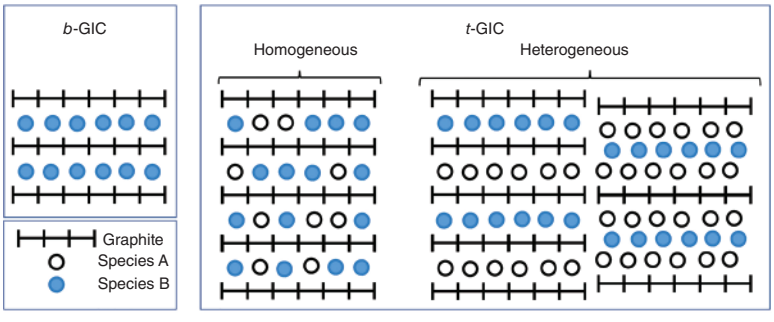

Figure 1.2 Classification of GICs into binary GICs (*b*-GICs) where a single species is intercalated into the graphite and ternary GICs (*t*-GICs) where two unique species are intercalated. The *t*-GICs can be further divided into homogeneous – where the two species are randomly distributed in the graphite – and heterogeneous, where the two intercalants are ordered in distinguishable layers. Source: Adapted from Ref. [19].

the structure evolves on a molecular scale. The difference is illustrated in Figure 1.2 as discussed by Solin [19]. The interesting point, however, is the fact that in some cases only the combination of two intercalants leads to GIC formation, while the individual intercalants do not intercalate on their own. Considering this, it easily becomes apparent that the chemistry of GICs is extremely rich and might be tailored by adding additional reactants. Possibly, a large number of GICs exist that have not been studied yet (Figure 1.2).

1.3 Graphite as Negative Electrode in LIBs and SIBs

1.3.1 Graphite in Lithium-Ion Batteries, Li-rich *b*-GICs

The development of carbon materials was essential for the success of LIBs. In the first commercial cells, disordered carbon had been applied as a negative electrode based on studies pioneered by Yoshino et al. from Asahi Kasai (Nobel Prize in 2019) [20]. Disordered carbons can be classified into hard and soft carbons. The difference between the two is that soft carbons can be transformed to graphite upon heat treatment as they are based on aromatic precursors. Hard carbons on the other hand exhibit such a large degree of disorder (large sp^3 content) that they cannot be transformed to graphite under practical conditions. The microstructure of disordered carbons is extremely complex and mainly depends on the carbonization temperature and the type of precursor used. These carbons usually contain larger amounts of foreign elements such as H, O, or N, which strongly influence the properties of the carbon as well. Due to the disorder, different mechanisms contribute to the storage of alkali metals like lithium and sodium in these materials. Compared to graphite, staging does not take place and the ion insertion takes place over a broader potential range leading to a more sloping voltage behavior [21]. The development of hard carbons for SIBs is frequently summarized in literature [22], see also the chapter on Hard Carbon. Despite the promise of disordered carbons, it is important to realize that it is graphite that is largely used for LIBs thanks to its so far better overall properties.

The theoretical capacity of graphite is 372 mAh g^{-1} (based on the LiC_6 stoichiometry) with around 360 mAh g^{-1} observed in commercial batteries. The reaction can be generalized as follows:

$$\mathrm{Li^+(solv)}_n(l) + x \cdot C(s) + \mathrm{e^-}(g) \overset{\text{intercalation}}{\rightleftarrows} \mathrm{LiC}_x(s) + n \cdot \mathrm{solv}(l) \tag{1.1}$$

LiC_x is a binary GIC. As mentioned, the reaction proceeds over several intermediate stages that can be followed by X-ray diffraction (XRD) [23]. For the final stage (stage I), x equals 6 [22a, 24]. The redox activity occurs largely between 0.05 and 0.2 V vs. Li^+/Li. The equation emphasizes the fact that Li^+ in the liquid electrolyte has a solvation shell that needs to be stripped during charge transfer. This is fundamentally different from the concept discussed in the next sections where the solvation shells (or parts of it) are co-intercalated into the graphite lattice.

Graphite was originally considered as impractical for LIBs because delamination of the graphite lattice took place during intercalation, e.g. when propylene carbonate was used as electrolyte solvent [25]. The use of ethylene carbonate as co-solvent was a breakthrough in solving this problem [26]. This solvent leads to a favorable surface layer on the graphite particles (solid electrolyte interphase, SEI) and therefore enables highly reversible intercalation/deintercalation of Li^+. Nowadays, the SEI is optimized by special additives and formation protocols. The concept of the SEI was introduced by E. Peled [27] and is frequently reviewed too. It is interesting to note that the lack of a suitable SEI so far prevents the use of Li as anode material for rechargeable batteries, though considerable efforts are undertaken to solve this problem [28].

1.3.2 Problems in Using Graphite in Sodium-Ion Batteries (The Lack of Na-rich *b*-GICs)

Because of the chemical similarity between lithium and sodium, the use of carbon materials in SIBs seems straight forward. While hard carbons show an appreciable Na storage capacity, the use of graphite was less successful for a long time. The reported capacity values were quite low, typically in the range of 20–40 mAh g^{-1}, i.e. Na-rich *b*-GICs did not form [29]. This was often explained by the larger size of the sodium ion ($r_{Na+} = 1.06$ Å vs. $r_{Li+} = 0.76$ Å); however, the even larger alkali metal ions seemed to have no difficulty forming *b*-GICs (KC_8, RbC_8, and CsC_8) [11b]. Thus, the size of the alkali metal ion is an insufficient descriptor for determining an ion's ability to intercalate into graphite.

Several theoretical studies addressing the lack of Na-rich *b*-GICs found that they are thermodynamically unfavorable [24c, 30]. Nobuhura et al. linked the positive formation energies in sodium-rich *b*-GICs with stretching, and subsequent destabilization, of the C—C bonds within the graphene sheets [24c], while Liu et al. found that among the alkali and alkali earth metals sodium and magnesium ions generally show the weakest binding to substrates, arising from the trends in the competing ionization energies and ion–substrate coupling [30a]. An important theoretical study was published by Moriwake et al. who suggested that Li (rather than Na) should be viewed as the exception within the series of alkali metal *b*-GICs. Following trends within the alkali metal, Li *b*-GICs should be unstable too; however, additional covalent bonding stabilizes the structure making the formation thermodynamically feasible [30b]. Similar conclusions were also reported by Lenchuk et al., supporting the argument that Na-rich GICs are thermodynamically unfavorable and it is lithium that breaks the trend among the alkali metals [30c].

1.3.3 Solution to Use Graphite in Sodium-Ion Batteries (Utilizing Na-rich *t*-GICs)

Due to the lack of Na-rich *b*-GICs, the use graphite in SIBs seemed not promising. In 2014, however, Jache and Adelhelm and Kim et al. independently reported on a reversible redox reaction [31]. In their studies, they replaced the conventional

carbonate-based electrolytes by ethers, this way obtaining storage capacities between 100 and 150 mAh g^{-1}. Although the specific capacity was inferior compared to hard carbons and a large volume expansion took place, the initial Coulombic efficiency (ICE), cycle life, and kinetics or the reaction was notably better. The underlying storage mechanism for the reaction is the formation of a *t*-GIC, which only took place in case ethers were used as electrolyte solvents. Like for *b*-GICs, several intermediate phases (stages) are observed during charging/discharging, which can be seen from Figure 1.3a and the derivative plot in Figure 1.3b. Intercalation starts just below 1 V vs. Na^+/Na after which characteristic steps occur (clearly visible in Figure 1.3b as peaks). A larger plateau occurs at ~0.6 V vs. Na^+/Na, representing a two-phase region, followed by a mainly pseudo-capacitive region down to 0 V vs. Na^+/Na.

The half-cell reaction for the formation of a *t*-GIC can be written as:

$$\mathrm{Na^+(solv)}_n + x \cdot \mathrm{C} + \mathrm{e^-} \overset{\text{intercalation}}{\rightleftarrows} \mathrm{Na(solv)}_n\mathrm{C}_x \tag{1.2}$$

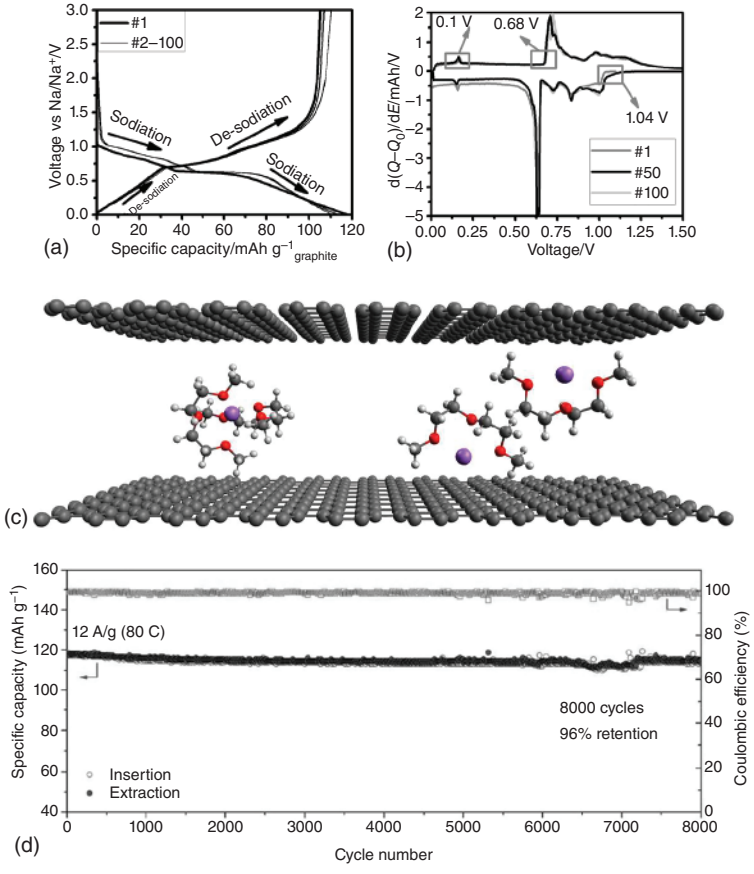

Figure 1.3 (a) The voltage profile of graphite in 1 M NaOTf in diglyme with the characteristic plateau at (b) c. 0.7 V vs. Na/Na^+. (c) Illustration of diglyme co-intercalated with sodium into graphite. (d) The reaction is highly reversible, showing 96% capacity retention after 8000 cycles. From [32]/with permission of American Chemical Society.

Compared to the formation of *b*-GICs (reaction Eq. (1.1)), where the solvation shell is completely stripped during charge transfer, here, the solvation shell is (partly) co-intercalated leading to a compound $Na(solv)_nC_x$ (Figure 1.3c). In other words, desolvation during charge transfer does not take place and the activation barrier for charge transfer becomes lower.

It is interesting to note that Na *t*-GICs have been prepared by chemical methods already since the 1950s with the main aim of exploring the structural variety of this materials class [12, 33]. A few electrochemical studies have been reported also, but it was the recently discovered unexpected reversibility of the reaction that lead to renewed interest of this reaction in the past few years. The reversibility is indeed surprising at first as the co-intercalation of solvent molecules was usually considered as quite problematic in LIB graphite electrodes, because the process lead to delamination of the graphite structure and therefore rapid electrode degradation. The use of ethers as electrolyte solvents, however, seems to overcome this problem. Interestingly, *t*-GIC formation with ethers also takes place in case of lithium, but the cycle life is inferior compared to sodium cells [31a]. A range of studies have been published on *t*-GIC formation in electrochemical cells in the meanwhile and has been recently summarized in reviews by Park et al. [34] and Li et al. [1c].

For diglyme as solvent, the electrochemical half-cell reaction can be written as:

$$\begin{aligned} &Na^+(diglyme)_n(l) + x \cdot C(s) + e^-(g) \overset{\text{intercalation}}{\rightleftarrows} \\ &\quad Na(diglyme)_nC_x(s) \;\; n = 1 \; or \; 2, \;\; x = 16 - 26 \end{aligned} \tag{1.3}$$

Experimental as well as theoretical results suggest that either one or two solvent molecules are being co-intercalated per sodium ion (see Figure 1.1c), and literature values for x range from 16 to 26 [31a, 32, 35]. For $x = 20$, the theoretical specific capacity becomes 112 mAh $g^{-1}_{(graphite)}$. Upon co-intercalation, a significant increase in the graphene layer spacing occurs, expanding from 3.35 Å up to 11.3–11.9 Å until a stage I compound has formed. The resulting large volume change is typically detrimental to the cycle life of electrodes [29e, 35a, c, 36]. Surprisingly, however, the graphite structure is preserved during cycling even at high rates and high current densities [36]. For example, over 8000 cycles [32] and current densities up to at least 30 A g^{-1} have been reported (Figure 1.3d). The high rate capability requires a fast diffusion, which is surprising considering the large size of the ion along with the co-intercalated solvent molecules. Nuclear magnetic resonance (NMR) studies indicate that the fast diffusion is enabled by an almost free rotation of the diglyme molecules (specifically in case of Na^+) [35b, 37]. A more detailed discussion on the NMR results can found in a review by Gotoh [38]. Finally, it is important to emphasize that the solvent required for the reaction has to be supplied from the electrolyte. This means that excess electrolyte is necessary. Considering Eq. (1.3) and assuming $n = 2$ and $x = 20$, the amount of electrolyte needed is 10.7 µl mAh^{-1} or 1.18 µl mg^{-1} (graphite) [39].

Overall, there are plenty of questions left unanswered related to the exact structure, composition, and dynamics of the reaction (e.g. diffusion of solvated ions in the lattice, charge transfer process, lattice changes, and so on). The following section

provides a more detailed discussion on this peculiar reaction and discusses factors that influence the electrode behavior.

1.4 Recent Development in Using Graphite for SIBs

This section discusses various aspects of co-intercalation reactions in SIBs. Various studies have been published in the past years that largely aim at understanding how the reaction is influenced by the electrolyte composition and the temperature. Moreover, the lattice and electrode expansion/shrinkage during cycling has been studied and diffusion properties were analyzed. An interesting aspect is also the question on whether the graphite surface is covered by and SEI or not. Here, we focus on the properties of the graphite electrode, i.e. results were obtained in half-cell geometry with Na as counter electrode. However, it should be also mentioned that graphite electrodes in SIBs were already successfully used in laboratory full cells too, e.g. paired with $Na_{1.5}VPO_{4.8}F_{0.7}$ [40], $Na_3V_2(PO_4)_3$ [41], $Na_{0.7}CoO_2$ [42], and activated carbon (hybrid capacitor) [43]. Moreover, finding low-cost graphite for SIBs becomes a topic of interest [41b, 44].

1.4.1 Lattice and Electrode Expansion During Cycling

During the electrochemical processes of ion intercalation, co-intercalation, or adsorption, the electrodes experience a structural change in the crystal lattice, causing a change in the volume of the electrode. If the continuous expansion and shrinkage of the electrodes during cycling causes significant mechanical stress, the cycle life of the battery can be greatly limited. Moreover, a large volume expansion limits the volumetric energy and power density of the system. Thus, as co-intercalation causes a great change in the spacing between graphene sheets, the volume expansion of the electrode is a topic of great importance in these systems.

To monitor the lattice changes during cycling, in situ/operando XRD can be carried out. Seidl et al. used operando XRD to study the staging behavior for mono-, di-, tri-, and tetraglyme and found that triglyme causes the smallest lattice expansion while also skipping the stage III compound. Overall, the interlayer spacings upon complete sodiation are between 11.59 and 12.01 Å [36]. Solvent effects were also studied by Jache et al. using postmortem XRD, with the same conclusion that triglyme caused the smallest lattice expansion, see Figure 1.4a [29e]. Another approach to study lattice changes is to use theoretical models. Density functional theory has been used to investigate the energetically most favorable distance between two graphene sheets with a solvated ion placed in between them, showing that the interlayer spacing increases from 3.35 to 11.3 Å, in good agreement with experimental results [45]. Therefore, a volume expansion of 240–250% is expected. Such a large volume change during ion storage is undesired of course. However, electrodes consist of many individual particles that are held together by a binder, and depending on the preparation method, the porosity of the electrode can be adjusted in a wide range. The porosity of lab electrodes typically varies between

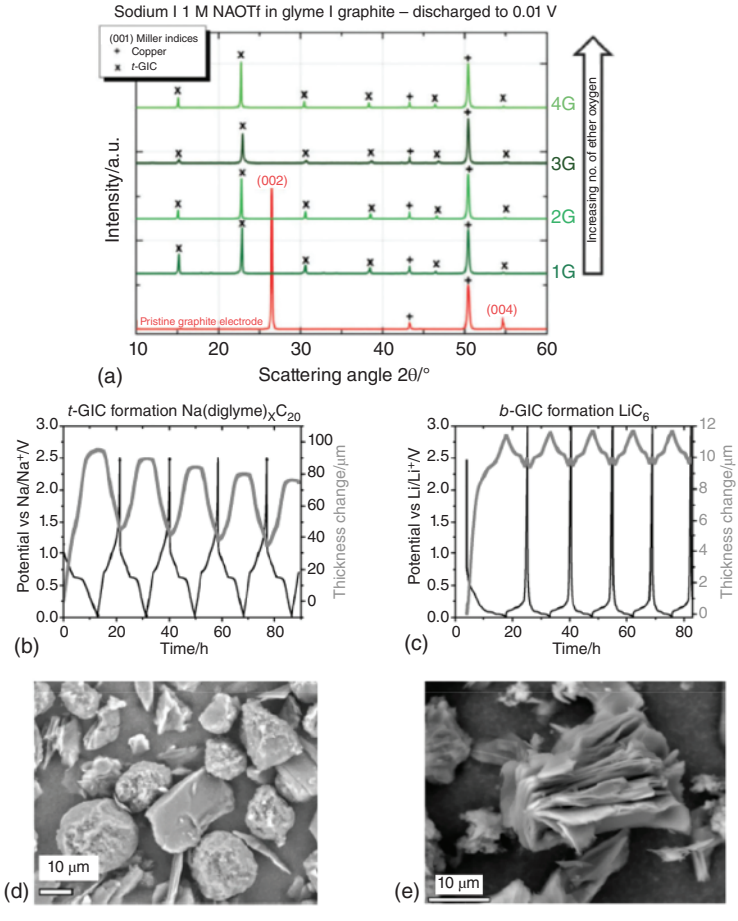

Figure 1.4 (a) XRD measurements showing the large shift in the lattice spacing during the co-intercalation reaction (Source: Adapted from Ref. [35d]); ECD is used to track the subsequent volume expansion, in which a sharp contrast can be seen between (b) a co-intercalation reaction and (c) an intercalation reaction. SEM images of (d) pristine graphite particles and (e) the exfoliated graphite after initial sodiation (Source: From [45]/with permission of John Wiley & Sons.)

30 and 70 vol%. The expansion/shrinkage of an electrode can be therefore quite different from what is expected from the changes of the crystal lattice.

The method of choice to study the expansion/shrinkage of electrodes during cell cycling is electrochemical dilatometry (ECD). ECD is often referred to as an in situ method, although the actual mode is operando. Measurements provide valuable information on how the composition and morphology of the electrode affects the overall volume changes – hopefully enabling a way to mitigate the large volume expansion. Typical ECD measurement results are shown in Figure 1.4b, c. The graphs show the first five cycles of a graphite electrode in a Na cell with ether electrolyte (diglyme, *t*-GIC formation) in comparison with a Li cell with

conventional carbonate electrolyte (EC:DMC, *b*-GIC formation). For the Na cell, the thickness of the electrode (initially about 50 µm) increases by almost 200% during initial sodiation. Subsequent desodiation leads to electrode shrinkage although not to the original value. Further cycling leads to periodic expansion and shrinkage (also called "breathing") of about 50 µm, i.e. a change of 100% compared to the initial electrode thickness. This is still large but much smaller compared to the changes of the crystal lattice.

For comparison, Figure 1.4 also shows ECD data for the formation of a *b*-GIC (LiC_6). Here the interlayer spacing during Li intercalation increases only by around 10% and consequently also the change in electrode thickness becomes much smaller compared to the formation of a *t*-GIC. For a comparable electrode (starting thickness of 50 µm), the electrode breathing for *b*-GIC formation only amounts to around 2 µm, or 4–6% (with at the same time an around 3× higher capacity!). The graphs also show that the first cycle is exceptional in both cells, i.e. the initial thickness change is much larger than in the subsequent cycles. Such an "activation" can be attributed to several phenomena but is likely due to particle restructuring and exfoliation. The exfoliation can be seen from scanning electron microscopy (SEM) images, see Figure 1.4d, e. While the pristine graphite particles are smooth and well defined, the particles exfoliate to platelets within the first cycle. The important point is, however, that delamination of the graphite does not take place, i.e. the graphene sheets are not separated. The platelets remain graphite crystals with an average crystal thickness of around 30 nm, and the crystallinity is preserved over several thousand cycles. This can be seen, e.g. from postmortem analysis or simply from the voltage profiles that maintain their characteristic shape over cycling. The initial large volume expansion seen in ECD captures the irreversible exfoliation process forming the platelets, while the breathing observed in subsequent cycles results from the reversible co-intercalation process into the platelet structure. The expansion in the first cycle also depends on the type of binder as shown by Escher et al. when comparing Polyvinylidene Fluoride (PVDF) and carboxymethyl cellulose (CMC) [46]. A comprehensive review of the ECD method is given in [47]. Overall, the large differences seen in ECD results between the Li and the Na cells are a direct indication for the different reaction mechanisms and the measurements correlate well with the XRD studies [31a].

1.4.2 Influence of the Electrolyte

Reaction Eq. (1.3) shows that the solvent becomes part of the redox reaction. This provides an opportunity to tailor the redox behavior of the graphite electrode. For instance, the redox potential can be shifted by around 200 mV using a series of glymes [29e, 48]. Mono-, di-, tri-, tetra-, and pentaglyme have been systematically investigated by several groups. Exceptions within the series of glymes are tri- and pentaglyme as they do not display a defined redox plateau at room temperature along with a lower capacity. In case of triglyme, this has been explained by an unfavorable coordination of the sodium ion [29e]. Pentaglyme is likely too viscous to enable better results at room temperature.

Due to their similarity with glymes, the crown ethers have also been investigated and shown to enable the co-intercalation reaction. Crown ether 4 (12-crown-4), crown ether 5 (15-crown-5), and crown ether 6 (18-crown-6) have been shown to co-intercalate at elevated temperatures although with limited success. A possible reason is that the crown ethers lack the structural flexibility required to form *t*-GICs. The most successful results were obtained for 18-crown-6 for which a reversible capacity close to 80 mAh g^{-1} was obtained at 60 °C [39]. The voltage profile shows large polarization and many steps indicating a complex storage mechanism with sluggish kinetics.

In contrast to the solvent, the anion does not take part in the co-intercalation process and hence does not affect the co-intercalation reaction. The anion, however, has an effect on the interfaces/interphases in the cell and therefore can have a strong impact on the electrochemical behavior. A systematic study on the influence of the conductive salt was performed by Goktas et al. [48]. Diglyme-based electrolytes containing NaOTf, $NaPF_6$, $NaClO_4$, NaFSI, and NaTFSI were compared. The study concluded that the salts can be ranked from best to worst in the following order NaOTf ≥ $NaPF_6$ > $NaClO_4$ > NaFSI ≫ NaTFSI. The reason for the poor behavior of NaTFSI is the instability at low potentials that causes side reactions at the graphite electrode and, in case of half-cell experiments, the Na counter electrode. The side reactions in case of NaTFSI (and partially also NaFSI) lead to excess discharge capacity, poor Coulomb efficiency, and poor cycle life. The side reactions also affect the dilatation of the electrode, where the thickness increases to greater values upon cycling along with trapping of ions in the graphite structure. The best results were obtained for $NaPF_6$ and NaOTf for which excellent cycle life and high Coulomb efficiency were obtained. The extent of side reactions was also followed by gas analysis, which clearly showed indication for continuous side reactions in case of NaTFSI and NaFSI.

Xu et al. systematically studied the influence of the salt concentration on the redox behavior [40]. Increasing the concentration of $NaPF_6$ from 0.05 to 3 M leads to a decrease in voltage. Only a minor influence is found in the lower concentration range from 0.05 to 1 M where the voltage changes only by 8 mV. A stronger impact is found in concentrated electrolytes from 1 to 3 M with a shift of approximately 100 mV.

Besides glymes, a few glyme derivatives, and some crown ethers [29e, 39], ethylenediamine (EN), as a co-solvent, is the only other solvent that has so far shown to have an effect on the co-intercalation behavior. Using ethylenediamine in a 1 : 1 ratio with diglyme lowers the voltage of the plateau as shown by Zhang et al. [49]. Escher et al. found the same for even smaller amounts (10 vol% EN) [46]. The addition of EN changes the voltage profile indicating that it actively participates in the reaction. The underlying redox reaction is not well understood, but both solvents (EN and diglyme) may co-intercalate together into the graphite lattice. This leads to a further increase in structural complexity and demonstrates another possibility of tailoring the properties of *t*-GICs. Interestingly, adding EN also significantly lowers the lattice and electrode expansion. The electrode breathing as

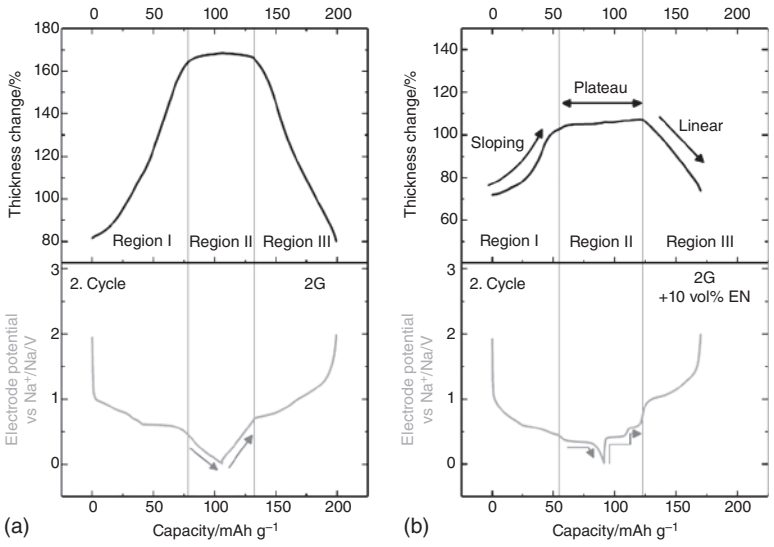

Figure 1.5 Voltage profiles and electrochemical dilatometry (ECD) data for *t*-GIC formation in Na cells with electrolytes containing only diglyme (2G) as solvent and diglyme + 10 vol% ethylenediamine (EN). The conductive salt is $NaPF_6$. The addition of EN changes the redox behavior as seen from the change in the voltage profile and significantly reduces the expansion/shrinkage (breathing) or the electrode. The graphs show the second cycle. Source: From [46]/John Wiley & Sons/CC BY 4.0.

measured by ECD only amounts to around 20%. A comparison of voltage profiles and ECD data with and without EN as co-solvent are shown in Figure 1.5 [46].

1.4.3 Influence of Temperature

The influence of temperature on the formation of *t*-GICs has been studied as well. Generally, the temperature influences the kinetic and thermodynamic properties of a reaction. From a thermodynamic point of view, the change of the cell voltage E with temperature depends on the reaction entropy according to $(\mathrm{d}E/\mathrm{d}T) = \Delta S/zF$. From a kinetic point of view, the rate constant k depends on temperature according to $k = \text{Const.} \cdot \exp(E_a/k_B T)$, with E_a being the activation energy. Systematic measurements by Goktas et al. between 25 and 85 °C showed that the reactions in mono-, di-, and tetraglyme are thermodynamically controlled, as the plateau redox potentials decrease linearly with increasing the temperature [39]. The same study showed a temperature coefficient of the redox potential of $-2.55 \pm 0.3\,\mathrm{mV\,K^{-1}}$, which can be used to calculate the entropy change of the reaction. The entropy change was also discussed by Xu et al., noting that the entropy change for *t*-GIC formation is larger compared to conventional intercalation reactions [28b]. This means that the redox potential of *t*-GIC reactions is comparably sensitive to temperature (although the absolute changes remain small within reasonable temperature ranges). As mentioned earlier, the use of tri- and pentaglyme as solvents leads to poor room temperature redox activity compared to mono-, di-, and tetraglyme. Temperature-dependent

studies revealed that this is a kinetic effect, and both solvents work well at slightly elevated temperature starting from around 40 °C [39]. Increasing the cell temperature can also promote side reactions that started when exceeding temperatures of 70–80 °C.

1.4.4 Physicochemical Properties

For battery electrolytes, two of the more important physicochemical properties are viscosity and ionic conductivity, and both properties are highly dependent on temperature. For glymes, the viscosity increases with the length of the glyme from 0.78 mPas (monoglyme) to 7.59 mPas (tetraglyme) at 20 °C. For monoglyme, the viscosity was only determined at 20 °C due to the high vapor pressure. The viscosity, however, for pentaglyme is much greater than the other glymes, with 186 mPas at 20 °C, but once the temperature is increased, the viscosity decreases sharply to 72.2 mPas (50 °C) all the way down to 22.4 mPas (80 °C). Although kinetic properties of electrode reactions depend on many parameters, low values of viscosity are favored [39]. The ionic conductivity of the electrolyte is critical for the battery. The diglyme-based electrolyte has a significantly higher conductivity than electrolytes based on mono-, tri-, tetra-, and pentaglyme and crown ethers. Using NaOTf, the ionic conductivity in diglyme is 4.47 mS cm^{-1} at 20 °C and increases to 5.91 mS cm^{-1} at 60 °C and 6.23 mS cm^{-1} at 80 °C, even at −30 °C, the conductivity is 1.59 mS cm^{-1}. The low freezing point of diglyme (−64 °C) is an advantage in view of low temperature battery operation. It is worth to mention that the ionic conductivity of triglyme-based electrolyte is particularly low at 20 °C, only having an ionic conductivity of 0.306 mS cm^{-1}; however, it quickly rises to 2.60 mS cm^{-1} at 60 °C all the way to 3.56 mS cm^{-1} at 80 °C [39]. Again, this might be connected with the unfavorable coordination between triglyme and the sodium ion [29e, 39].

Several Raman spectroscopy studies have shown how the G, D, and D′ bands are affected by the co-intercalation process [31b, 32, 41a, 51]. Pristine graphite displays a strong G band and a weak D band, characteristic of the strong sp^2-hybridized C—C bonds. Upon co-intercalation the intensity of the D band increases greatly, and the D′ band emerges, indicating sp^3 defects and the formation of a staged GIC, as shown in Figure 1.6 [31b, 41a, 51]. The excellent cyclability is again manifested by the Raman measurements, as barely any changes in the structure are observed over 8000 cycles [32].

Besides showing an impressive capacity retention of 96% after 8000 cycles and the ability to operate at 65% of capacity at a current density of 30 A g^{-1}, i.e. the cell can be fully charged in 12.5 seconds, Cohn et al. investigated the diffusion of solvated sodium ions using the galvanostatic intermittent cycling technique and attributed the great rate capabilities to the fast diffusion of the sodium ions in the electrode material [32]. Similarly, Jung et al. made theoretical investigations of the diffusion of solvated sodium ions between the graphene layers and found, surprisingly, that the diffusion coefficients were an order of magnitude higher for the solvated sodium ions compared with bare sodium or lithium ions, i.e. *t*-GICs might be especially suited for high-power batteries [35c].

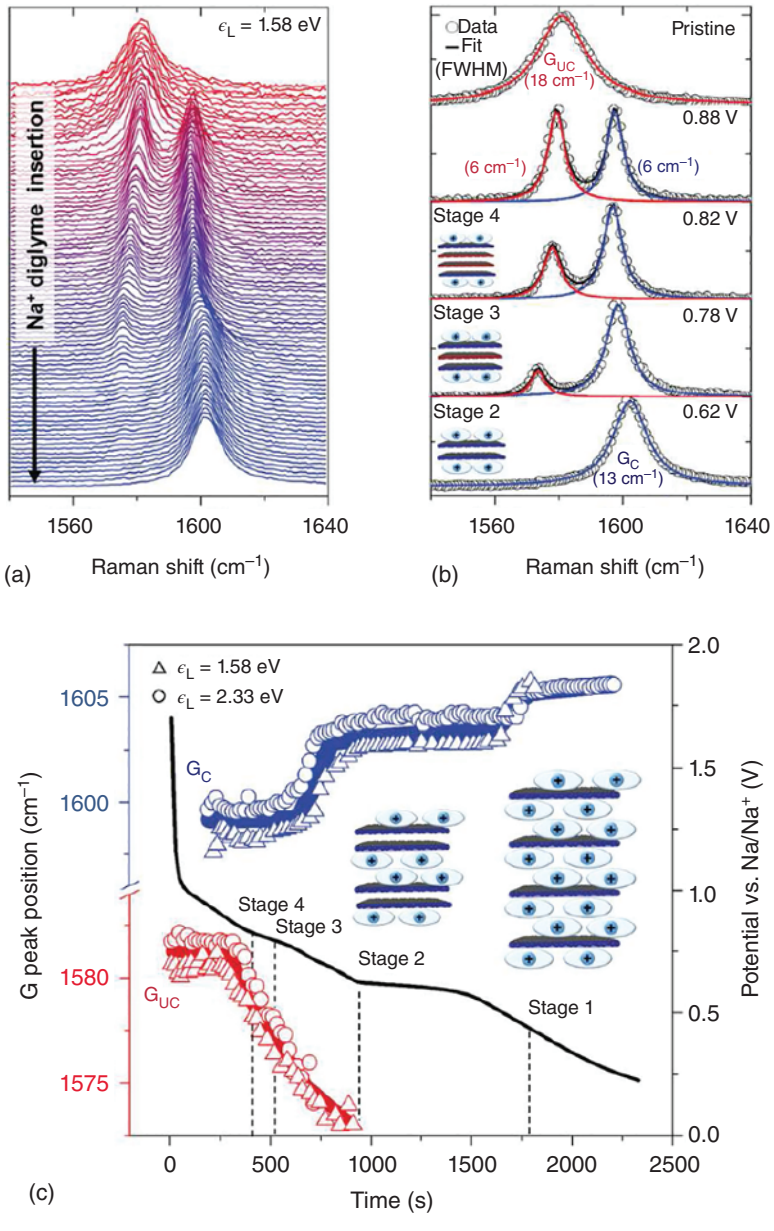

Figure 1.6 (a) In situ Raman spectra showing the highly ordered staging reaction with (b) selected spectra and Lorentzian fits of components. (c) Tracking the positions of the Raman G peak components during the electrochemical intercalation reaction with the corresponding Galvanostatic discharge (~0.2 A g^{-1}) profile shown with respect to right *y*-axis (black line). Source: From [32]/with permission of American Chemical Society.

1.4.5 Solid Electrolyte Interphase (SEI)

The SEI has been thoroughly studied for LIBs. The SEI directly affects the battery performance, and its formation and characteristics are hence of great importance. Ideally, the SEI is electronically insulating, ionically conducting, chemically and mechanically stable (but flexible enough to follow the volume changes during cycling), and it should form within the initial cycles such that the system quickly stabilizes [52]. From a classical perspective, the SEI also prevents any solvent co-intercalation. Without doubt, a reversible graphite electrode based on solvent co-intercalation questions this traditional concept of an SEI. Whether or not an SEI exists in the case of reversible *t*-GICs electrodes is therefore controversially discussed. Especially, the fact that the reaction can be so fast indicates an extremely low charge transfer resistance for the solvated Na^+, which, at the same time, would require an SEI-free (or nearly SEI-free) interface. Several studies therefore addressed the characteristics of the SEI. While Maibach et al. [52] and Wang et al. [53] reported on an existing SEI, our group and the Kang group concluded that the co-intercalation reaction requires an "SEI-free" interface that was supported by transmission electron microscopy (TEM), X-ray photoelectron spectroscopy (XPS), and Online electrochemical mass spectroscopy (OEMS) studies [45, 54]. None of the analytical tools is perfect, and analyzing SEIs on battery electrodes is chronically difficult for various reasons. In some cases, however, the different findings can be explained by different experimental conditions. Wang et al. used a graphite electrode with a large fraction of super-P as additive, and the studies by Maibach et al. and Goktas et al. used different electrolytes (NaFSI in tetraglyme vs. NaOTf in diglyme). Our own findings indicate that NaFSI causes additional side reactions [48] that may artificially lead to an excessive SEI formation. Moreover, an SEI may also form on conductive additives that may mask the graphite particles. A similar problem arises from the binder that is typically used to prepare electrodes. An indication of excessive side reactions can be seen from the Coulomb efficiencies that are low for the electrodes with large amounts of conductive additive and NaFSI-containing electrolytes.

Figure 1.7 shows TEM images of graphite particles after electrochemical cycling. The left image shows the results for a Li cell with carbonate electrolyte (*b*-GIC formation) for which an SEI can be observed. The right image shows results for a Na cell after cycling in a diglyme electrolyte (*t*-GIC formation). When cycling this electrode, neither binder nor conductive additive was used. In this case, an SEI is not visible. Similar results were reported by Kim et al. who could not find an SEI by TEM (and XPS) [54]. As mentioned, analysis is challenging and the common techniques to study the SEI such as XPS and TEM are postmortem techniques that require a sample transfer and sample preparation that may cause surface reactions that may be misinterpreted as an SEI. On the other hand, too intense washing of the electrodes during sample preparation may wash off the SEI. Moreover, contamination of the graphite surface may also arise from reactions of the electrolyte with the counter electrode (cross-talk).

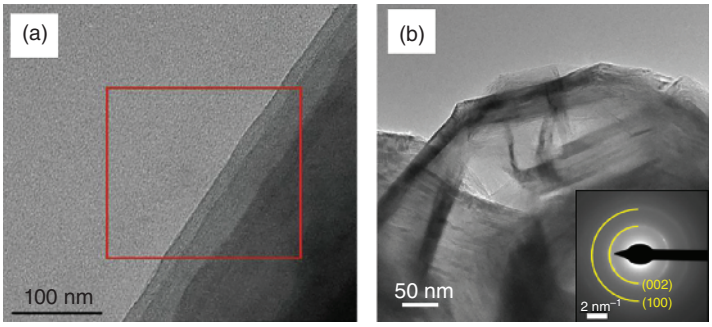

Figure 1.7 (a) TEM images of fresh graphite and SEI on graphite anodes cycled to four cutoff voltages in 1.2 M $LiPF_6$/EC during first charge (Source: From [55]/with permission of American Chemical Society); (b) TEM and HRTEM images of the graphite particles after cycling in electrolyte solutions of 1 M NaOTf in diglyme (end of fifth cycle, desodiated state). Insets: Selected area electron diffraction (SAEDs) patterns for areas; the semi-circles indicate the expected positions for graphite interplanar distances. (Source: From [48]/with permission of American Chemical Society).

Overall, the charge transfer of solvated ions into graphite is quite intriguing. Whether or not an SEI exists in case of reversible *t*-GIC formation remains a matter of debate. Related to that, theoretical studies suggest that diglyme can be indeed stable at low potentials that may prevent SEI formation [56].

1.4.6 Increasing the Capacity

A major limitation of using graphite as electrode in SIBs is the limited capacity, which still remains at around 110 mAh g^{-1} for the *t*-GIC formation. This value is low for battery electrodes (should be $\gg$150 mAh g^{-1}) but high compared to capacitive electrodes, which indicates that *t*-GIC formation may be more suited to design high-power electrodes, e.g. also for hybrid capacitors. A higher capacity could be obtained by finding new Na *t*-GICs in which more sodium can be stored. The attempts so far, however, were not successful. A more practical approach to increase the capacity is to add metals. For LIBs, it is well known that small amounts of silicon can be added to graphite electrodes in order to increase the capacity. The general downside of high-capacity metals such as Si or Sn is that they show an extremely large volume expansion/shrinkage that leads to poor cycle life, so a careful optimization of the electrode and metal content is required. Si so far does not show good properties as anode in SIBs, but promising results were obtained for Sn that shows a theoretical capacity of 847 mAh g^{-1} for the formation of $Na_{3.75}Sn$ [57]. The theoretical volume expansion of Sn during complete sodiation is around 430% [58]. But for a carbon/Sn composite, the expansion on the electrode level can be much smaller. For example, Palaniselvam et al. found an expansion of 14% for a composite containing 58 wt% Sn and 42 wt% hard carbon [59]. Our group therefore also added small amounts of Sn to a graphite electrode and studied the impact on the Na storage behavior [43]. For an electrode containing 17 wt% Sn and 83 wt% graphite, the capacity reached 223 mAh g^{-1}, i.e. roughly doubling the

capacity compared to the pure graphite electrode. The ICE remained high at 90%, and the electrode showed a high-capacity retention for at least 2200 cycles. While the additional tin doubles the capacity, its contribution to the electrode expansion is negligible (~3%). Due to the high rate capability of the reaction, the electrode was tested as anode in a Na-ion hybrid capacitor (with an activated carbon as cathode). Excellent long-term cyclability with 80% of the original capacity after 8000 cycles were obtained. Based on the mass of the electrodes, the cell delivered an energy density 93 Wh kg^{-1} of and a power density of 7.8 kW kg^{-1}.

1.5 Outlook

Even though the formation of sodium-glyme *t*-GICs has gathered attention in the past few years, several questions are still left open for future research. First of all, the fundamental question of what combination of properties of the solvents, ions, and electrode material that enable these highly reversible co-intercalation and charge transfer processes remains unanswered and largely unaddressed. The desolvation energy, however, has been identified as a critical quantity, but a very limited set of solvents have been investigated in this regard [35d]. In fact, as the exact stoichiometry of the co-intercalation process in glyme-based electrolytes and graphite is unknown, more thorough and detailed investigations are probably needed before a fundamental understanding of the phenomenon can be established. Once such an understanding is achieved, it is possible that several new systems operating by the co-intercalation mechanism can be found; in fact, there are several studies on using potassium and di- or even trivalent cations [34].

Several studies have argued, or asserted, that a single diglyme molecule is brought along the sodium ion, and thus partial desolvation occurs before the ion enters the active material [28b, 35a, c, d]. For instance, one study measured the mass change of the graphite electrode along with energy dispersive X-ray spectroscopy and found that there is one solvent per cation [35a], and several theoretical studies have looked at a single solvent around the sodium ion [35b, 45]. Similarly, several studies have argued or, again, asserted, that two diglyme solvents are brought along the sodium ion, and hence no desolvation occurs in the charge transfer process, and theoretical studies have seen excellent agreement between the XRD measured graphene layer spacing and the computed spacing when the sodium ion is solvated by two diglymes [35b, 37, 45]. Two NMR studies found that the solvation shell remains intact with two diglyme molecules around the sodium ion in the graphite host, along with additional free diglyme molecules [35b, 37]. Moreover, one of the NMR studies revealed that the sodium solvation shells interact more weakly with the graphite than the lithium counterparts, allowing for faster diffusion of sodium ions [37]. Needless to say, as the research community is divided on what exactly enters the graphite galleries, more research is needed before the question can be settled.

As stated previously, several studies have investigated the SEI in these systems, but the results remain inconclusive, possibly due to the studied systems not being identical, and thus the existence, and, if so, the characteristics of the SEI

is still left unanswered. But, it is clear that the great rate capabilities cannot be achieved without the interface being highly permeable for entire solvation shells. Practical questions to be addressed in the future also relate to realistic full cells with minimized electrolyte volume and multilayers where the large breathing may lead to mechanical problems. It is therefore especially desirable to find Na-rich *t*-GICs with higher capacity but at the same time smaller lattice expansion. A more rational development would be enabled by a better understanding of the complex interactions between the graphite lattice, the Na ions, and the co-intercalated solvent molecules. A key advantage of Na *t*-GICs for practical applications so far seems the fast in-plane diffusion that could enable high-power devices.

References

1 (a) (1990). *Graphite Intercalation Compounds I*. Berlin: Springer-Verlag. (b) Inagaki, M. (1989). Applications of graphite intercalation compounds. *Journal of Materials Research* 4: 1560–1568. (c) Li, Y., Lu, Y., Adelhelm, P. et al. (2019). Intercalation chemistry of graphite: alkali metal ions and beyond. *Chemical Society Reviews* 48: 4655–4687. (d) Hérold, C. and Lagrange, P. (2006). Intercalation reactions into graphite: a two-dimensional chemistry; Les reactions d'intercalation dans le graphite. Une chimie bidimensionnelle. *Actualite Chimique* 33–37. (e) Zhang, M., Song, X., Ou, X., and Tang, Y. (2019). Rechargeable batteries based on anion intercalation graphite cathodes. *Energy Storage Materials* 16: 65–84. (f) Placke, T., Heckmann, A., Schmuch, R. et al. (2018). Perspective on performance, cost, and technical challenges for practical dual-ion batteries. *Joule* 2: 2528–2550. (g) Xu, J., Dou, Y., Wei, Z. et al. (2017). Recent progress in graphite intercalation compounds for rechargeable metal (Li, Na, K, Al)-ion batteries. *Advanced Science* 4: 1700146.

2 (a) Salvatore, M., Carotenuto, G., De Nicola, S. et al. (2017). Synthesis and characterization of highly intercalated graphite bisulfate. *Nanoscale Research Letters* 12: 167. (b) Rüdorff, W. (1959). Graphite intercalation compounds. *Advances in Inorganic Chemistry and Radiochemistry* 1: 223–266.

3 Yazami, R. and Touzain, P. (1983). A reversible graphite-lithium negative electrode for electrochemical generators. *Journal of Power Sources* 9: 365–371.

4 Schafhäutl, C. (1840). *Journal für praktische Chemie* 21: 129–157.

5 Brodie, B. (1855). *Annals de Chemie et de Physique* 45: 351–352.

6 Rüdorff, W. and Hofmann, U. (1938). *Zeitschrift für anorganische und allgemeine Chemie* 238: 1–50.

7 (a) Guerard, D. and Herold, A. (1975). Intercalation of lithium into graphite and other carbons. *Carbon* 13: 337–345. (b) Sole, C., Drewett, N.E., and Hardwick, L.J. (2014). In situ Raman study of lithium-ion intercalation into microcrystalline graphite. *Faraday Discussions* 172: 223–237. (c) Winter, M., Besenhard, J.O., Spahr, M.E., and Novák, P. (1998). Insertion electrode materials for rechargeable lithium batteries. *Advanced Materials* 10: 725–763. (d) Senyshyn, A., Dolotko, O., Mühlbauer, M.J. et al. (2013). Lithium intercalation into graphitic carbons

revisited: experimental evidence for twisted bilayer behavior. *Journal of The Electrochemical Society* 160: A3198–A3205. (e) Schweidler, S., de Biasi, L., Schiele, A. et al. (2018). Volume changes of graphite anodes revisited: a combined operando x-ray diffraction and in situ pressure analysis study. *The Journal of Physical Chemistry C* 122: 8829–8835.

8 Daumas, N. and Herold, A. (1969). *Comptes Rendus des Seances de l'Academie des Sciences, Serie C. Sciences Chimiques*.

9 (a) Gavilán-Arriazu, E.M., Pinto, O.A., López de Mishima, B.A. et al. (2018). The kinetic origin of the Daumas-Herold model for the Li-ion/graphite intercalation system. *Electrochemistry Communications* 93: 133–137. (b) Krishnan, S., Brenet, G., Machado-Charry, E. et al. (2013). Revisiting the domain model for lithium intercalated graphite. *Applied Physics Letters* 103: 251904. (c) Mathiesen, J.K., Johnsen, R.E., Blennow, A.S., and Norby, P. (2019). Understanding the structural changes in lithiated graphite through high-resolution operando powder X-ray diffraction. *Carbon* 153: 347–354.

10 Dimiev, A.M., Shukhina, K., Behabtu, N. et al. (2019). Stage transitions in graphite intercalation compounds: role of the graphite structure. *The Journal of Physical Chemistry C* 123: 19246–19253.

11 (a) Brandt, N.B., Chudinov, S.M., and Ponomarev, Y.G. (1988). *Modern Problems in Condensed Matter Sciences*,Chapter 10, vol. 20, 197–321. Elsevier. (b) Dresselhaus, M.S. and Dresselhaus, G. (2002). *Advances in Physics* 51: 1–186.

12 Zabel, H. and Solin, S. (1990). *Graphite Intercalation Compounds I, Structure and Dynamics*, vol. 14. Springer Series in Materials Science.

13 (a) Nayak, P.K., Yang, L., Brehm, W., and Adelhelm, P. (2018). From lithium-ion to sodium-ion batteries: advantages, challenges, and surprises. *Angewandte Chemie International Edition* 57: 102–120. (b) Hosaka, T., Kubota, K., Hameed, A.S., and Komaba, S. (2020). Research development on K-ion batteries. *Chemical Reviews* 120: 6358–6466.

14 (a) Das, S.K., Mahapatra, S., and Lahan, H. (2017). Aluminium-ion batteries: developments and challenges. *Journal of Materials Chemistry A* 5: 6347–6367. (b) Elia, G.A., Marquardt, K., Hoeppner, K. et al. (2016). An overview and future perspectives of aluminium batteries. *Advanced Materials* 28: 7564–7579.

15 Sui, Y., Liu, C., Masse, R.C. et al. (2020). Dual-ion batteries: the emerging alternative rechargeable batteries. *Energy Storage Materials* 25: 1–32.

16 Fauchard, M., Cahen, S., Lagrange, P. et al. (2019). Overview on the intercalation of gold into graphite. *Carbon* 145: 501–506.

17 Zhang, C., Ma, J., Han, F. et al. (2018). Strong anchoring effect of ferricchloride-graphite intercalation compounds (FeCl 3-GICs) with tailored epoxy groups for high-capacity and stable lithium storage. *Journal of Materials Chemistry A* 6: 17982–17993.

18 Li, Z., Zhang, C., Han, F. et al. (2020). Towards high-volumetric performance of Na/Li-ion batteries: a better anode material with molybdenumpentachloride–graphite intercalation compounds (MoCl5-GICs). *Journal of Materials Chemistry A* 8: 2430–2438.

19 Solin, S.A. (1986). Ternary graphite intercalation compounds. In: *Intercalation Layered Materials* (ed. M.S. Dresselhaus), 291–300. Springer.

20 (a) Blomgren, G.E. (2016). The development and future of lithium ion batteries. *Journal of The Electrochemical Society* 164: A5019–A5025. (b) Yoshino, A., Sanechika, K., and Nakajima, T. (1987). US Patent 4,668,595A.

21 Stevens, D.A. and Dahn, J.R. (2001). The mechanisms of lithium and sodium insertion in carbon materials. *Journal of The Electrochemical Society* 148: A803.

22 (a) Yabuuchi, N., Kubota, K., Dahbi, M., and Komaba, S. (2014). Research development on sodium-ion batteries. *Chemical Reviews* 114: 11636–11682. (b) Irisarri, E., Ponrouch, A., and Palacin, M.R. (2015). Hard carbon negative electrode materials for sodium-ion batteries. *Journal of The Electrochemical Society* 162: A2476–A2482. (c) Dou, X., Hasa, I., Saurel, D. et al. (2019). Hard carbons for sodium-ion batteries: structure, analysis, sustainability, and electrochemistry. *Materials Today* 23: 87–104. (d) Xie, F., Xu, Z., Guo, Z., and Titirici, M.-M. (2020). Hard carbons for sodium-ion batteries and beyond. *Progress in Energy* 2: 042002.

23 (a) Dahn, J.R. (1991). Phase diagram of LixC6. *Physical Review B: Condensed Matter* 44: 9170–9177. (b) Ohzuku, T., Iwakoshi, Y., and Sawai, K. (1993). Formation of lithium-graphite intercalation compounds in nonaqueous electrolytes and their application as a negative electrode for a lithium ion (shuttlecock) cell. *Journal of The Electrochemical Society* 140: 2490–2498.

24 (a) Charlier, A., Charlier, M.F., and Fristot, D. (1989). Binary graphite intercalation compounds. *Journal of Physics and Chemistry of Solids* 50: 987–996. (b) Nobuhara, K., Nakayama, H., Nose, M. et al. (2013). First-principles study of alkalimetal-graphite intercalation compounds. *Journal of Power Sources* 243: 585–587.

25 (a) Fong, R., Sacken, U.Y., and Dahn, J.R. (1990). Studies of lithium intercalation into carbons using nonaqueous electrochemical cells. *Journal of The Electrochemical Society* 137: 2009–2013. (b) Dey, A.N. and Sullivan, B.P. (1970). The electrochemical decomposition of propylene carbonate on graphite. *Journal of Electrochemical Society* 117: 222–224.

26 (a) Xu, K. (2019). A long journey of lithium: from the big bang to our smartphones. *Energy & Environmental Materials* 2: 229–233. (b) Winter, M., Barnett, B., and Xu, K. (2018). Before Li ion batteries. *Chemical Reviews* 118: 11433–11456.

27 (a) Peled, E. (1979). The electrochemical behavior of alkali and alkaline earth metals in nonaqueous battery systems—the solid electrolyte interphase model. *Journal of The Electrochemical Society* 126: 2047. (b) Peled, E., Golodnitsky, D., and Ardel, G. (1997). Advanced model for solid electrolyte interphase electrodes in liquid and polymer electrolytes. *Journal of Electrochemical Society* 144: L208–L210. (c) Peled, E. and Menkin, S. (2017). SEI: past, present and future. *Journal of The Electrochemical Society* 164: A1703–A1719.

28 (a) Krauskopf, T., Richter, F.H., Zeier, W.G., and Janek, J. (2020). Physicochemical concepts of the lithium metal anode in solid-state batteries. *Chemical Reviews* 120: 7745–7794. (b) Fang, C., Wang, X., and Meng, Y.S. (2019). Key issues

hindering a practical lithium-metal anode. *Trends in Chemistry* 1: 152–158. (c) Zhang, X.-Q., Cheng, X.-B., and Zhang, Q. (2018). Advances in interfaces between Li metal anode and electrolyte. *Advanced Materials Interfaces* 5: 1701097. (d) Li, S., Jiang, M., Xie, Y. et al. (2018). Developing high-performance lithium metal anode in liquid electrolytes: challenges and progress. *Advanced Materials* 30: 1706375. (e) Yu, X. and Manthiram, A. (2018). Electrode-electrolyte interfaces in lithium-based batteries. *Energy & Environmental Science* 11: 527–543. (f) Nair, J.R., Imholt, L., Brunklaus, G., and Winter, M. (2019). Lithium metal polymer electrolyte batteries: opportunities and challenges. *The Electrochemical Society Interface* 28: 55–61.

29 (a) Wenzel, S., Hara, T., Janek, J., and Adelhelm, P. (2011). Room-temperature sodium-ion batteries: Improving the rate capability of carbon anode materials by templating strategies. *Energy & Environmental Science* 4: 3342. (b) Slater, M.D., Kim, D., Lee, E., and Johnson, C.S. (2013). Sodium-ion batteries. *Advanced Functional Materials* 23: 947–958. (c) Ge, P. and Fouletier, M. (1988). Electrochemical intercalation of sodium in graphite. *Solid State Ionics* 28–30: 1172–1175. (d) Cabello, M., Chyrka, T., Klee, R. et al. (2017). Treasure Na-ion anode from trash coke by adept electrolyte selection. *Journal of Power Sources* 347: 127–135. (e) Jache, B., Binder, J.O., Abe, T., and Adelhelm, P. (2016). A comparative study on the impact of different glymes and their derivatives as electrolyte solvents for graphite co-intercalation electrodes in lithium-ion and sodium-ion batteries. *Physical Chemistry Chemical Physics* 18: 14299–14316.

30 (a) Liu, Y., Merinov, B.V., and Goddard, W.A. 3rd, (2016). Origin of low sodium capacity in graphite and generally weak substrate binding of Na and Mg among alkali and alkaline earth metals. *Proceedings of the National Academy of Sciences* 113: 3735–3539. (b) Moriwake, H., Kuwabara, A., Fisher, C.A.J., and Ikuhara, Y. (2017). Why is sodium-intercalated graphite unstable? *RSC Advances* 7: 36550–36554. (c) Lenchuk, O., Adelhelm, P., and Mollenhauer, D. (2019). New insights into the origin of unstable sodium graphite intercalation compounds. *Physical Chemistry Chemical Physics* 21: 19378–19390. (d) Wang, Z., Selbach, S.M., and Grande, T. (2014). Van der Waals density functional study of the energetics of alkali metal intercalation in graphite. *RSC Advances* 4: 4069–4079.

31 (a) Jache, B. and Adelhelm, P. (2014). Use of graphite as a highly reversible electrode with superior cycle life for sodium-ion batteries by making use of co-intercalation phenomena. *Angewandte Chemie International Edition* 53: 10169–10173. (b) Kim, H., Hong, J., Park, Y.-U. et al. (2015). Sodium storage behavior in natural graphite using ether-based electrolyte systems. *Advanced Functional Materials* 25: 534–541.

32 Cohn, A.P., Share, K., Carter, R. et al. (2016). Ultrafast solvent-assisted sodium ion intercalation into highly crystalline few-layered graphene. *Nano Lett* 16: 543–548.

33 (a) Solin, S.A. and Zabel, H. (1988). The physics of ternary graphite intercalation compounds. *Advances in Physics* 37: 87–254. (b) Lagrange, P., Bendriss-Rerhrhaye, A., and Mcrae, J.F.M.A.E. (1985). Synthesis and electrical

properties of some new ternary graphite intercalation compounds. *Synthetic Metals* 12: 201–206.

34 Park, J., Xu, Z.-L., and Kang, K. (2020). Solvated ion intercalation in graphite: sodium and beyond. *Frontiers in Chemistry* 8: 432–432.

35 (a) Kim, H., Hong, J., Yoon, G. et al. (2015). Sodium intercalation chemistry in graphite. *Energy & Environmental Science* 8: 2963–2969. (b) Gotoh, K., Maruyama, H., Miyatou, T. et al. (2016). Structure and dynamic behavior of sodium–diglyme complex in the graphite anode of sodium ion battery by 2H nuclear magnetic resonance. *The Journal of Physical Chemistry C* 120: 28152–28156. (c) Jung, S.C., Kang, Y.J., and Han, Y.K. (2017). Origin of excellent rate and cycle performance of Na±solvent cointercalated graphite vs. poor performance of Li±solvent case. *Nano Energy* 34: 456–462. (d) Yoon, G., Kim, H., Park, I., and Kang, K. (2016). Conditions for reversible Na intercalation in graphite: theoretical studies on the interplay among questions, solvent, and graphite host. *Advanced Energy Materials* 1601519. (e) Kim, H., Yoon, G., Lim, K., and Kang, K. (2016). A comparative study of graphite electrodes using the co-intercalation phenomenon for rechargeable Li, Na and K batteries. *Chemical Communiations* 52: 12618–12621.

36 Seidl, L., Bucher, N., Chu, E. et al. (2017). Intercalation of solvated Na-ions into graphite. *Energy & Environmental Science* 10.

37 Leifer, N., Greenstein, M.F., Mor, A. et al. (2018). NMR-detected dynamics of sodium co-intercalation with diglyme solvent molecules in graphite anodes linked to prolonged cycling. *The Journal of Physical Chemistry C* 122: 21172–21184.

38 Gotoh, K. (2021). ^{23}Na solid-state NMR analyses for Na-ion batteries and materials. *Batteries & Supercaps* 4: 1267–1278.

39 Goktas, M., Akduman, B., Huang, P. et al. (2018). Temperature-induced activation of graphite co-intercalation reactions for glymes and crown ethers in sodium-ion batteries. *The Journal of Physical Chemistry C* 122: 26816–26824.

40 Xu, Z.-L., Yoon, G., Park, K.-Y. et al. (2019). Tailoring sodium intercalation in graphite for high energy and power sodium ion batteries. *Nature Communications* 10: 2598.

41 Zhu, Z., Cheng, F., Hu, Z. et al. (2015). Highly stable and ultrafast electrode reaction of graphite for sodium ion batteries. *Journal of Power Sources* 293: 626–634.

42 Hasa, I., Dou, X., Buchholz, D. et al. (2016). A sodium-ion battery exploiting layered oxide cathode, graphite anode and glyme-based electrolyte. *Journal of Power Sources* 310: 26–31.

43 Palaniselvam, T., Babu, B., Moon, H. et al. (2021). Tin-containing graphite for sodium-ion batteries and hybrid capacitors. *Batteries & Supercaps* 4: 173–182.

44 (a) Laziz, N.A., Abou-Rjeily, J., Darwiche, A. et al. (2018). Li-and Na-ion storage performance of natural graphite via simple flotation process. *Journal of Electrochemical Science and Technology* 9: 320–329. (b) Liu, K., Yang, S., Luo, L. et al. (2020). From spent graphite to recycle graphite anode for high-performance lithium ion batteries and sodium ion batteries. *Electrochimica Acta* 356: 136856.

45 Goktas, M., Bolli, C., Berg, E.J. et al. (2018). Graphite as cointercalation electrode for sodium-ion batteries: electrode dynamics and the missing solid electrolyte interphase (SEI). *Advanced Energy Materials* 8: 1702724.

46 Escher, I., Kravets, Y., Ferrero, G.A. et al. (2021). Strategies for alleviating electrode expansion of graphite electrodes in sodium-ion batteries followed by in situ electrochemical dilatometry. *Energy Technology* 9: 2000880.

47 Escher, I., Hahn, M., Ferrero, G.A., and Adelhelm, P. (2022). A practical guide for using electrochemical dilatometry as operando tool in battery and supercapacitor research. *Energy Technology* 2101120.

48 Goktas, M., Bolli, C., Buchheim, J. et al. (2019). Stable and unstable diglyme-based electrolytes for batteries with sodium or graphite as electrode. *Applied Materials and Interfaces* 11: 32844–32855.

49 Zhang, H., Li, Z., Xu, W. et al. (2018). Pillared graphite anodes for reversible sodiation. *Nanotechnology* 29: 325402.

50 Guan, Z., Shen, X., Yu, R. et al. (2016). Chemical intercalation of solvated sodium ions in graphite. *Electrochimica Acta* 222: 1365–1370.

51 Xu, K. (2014). Electrolytes and interphases in Li-ion batteries and beyond. *Chemical Reviews* 114: 11503–11618.

52 Maibach, J., Jeschull, F., Brandell, D. et al. (2017). Surface layer evolution on graphite during electrochemical sodium-tetraglyme cointercalation. *ACS Applied Materials & Interfaces* 9: 12373–12381.

53 Wang, Z., Yang, H., Liu, Y. et al. (2020). Analysis of the stable interphase responsible for the excellent electrochemical performance of graphite electrodes in sodium-ion batteries. *Small* 16: 2003268.

54 Kim, H., Lim, K., Yoon, G. et al. (2017). Exploiting lithium–ether co-intercalation in graphite for high-power lithium-ion batteries. *Advanced Energy Materials* 7: 1700418.

55 Nie, M., Chalasani, D., Abraham, D.P. et al. (2013). Lithium ion battery graphite solid electrolyte interphase revealed by microscopy and spectroscopy. *The Journal of Physical Chemistry C* 117: 1257–1267.

56 Westman, K., Dugas, R., Jankowski, P. et al. (2018). Diglyme based electrolytes for sodium-ion batteries. *ACS Applied Energy Materials* 1: 2671–2680.

57 (a) Ellis, L.D., Hatchard, T.D., and Obrovac, M.N. (2012). Reversible insertion of sodium in tin. *Journal of The Electrochemical Society* 159: A1801–A1805. (b) Li, Z., Ding, J., and Mitlin, D. (2015). Tin and tin compounds for sodium ion battery anodes: phase transformations and performance. *Accounts of Chemical Research* 48: 1657–1665.

58 Chevrier, V.L. and Ceder, G. (2011). Challenges for Na-ion negative electrodes. *Journal of The Electrochemical Society* 158: A1011.

59 Palaniselvam, T., Goktas, M., Anothumakkool, B. et al. (2019). Sodium storage and electrode dynamics of tin-carbon composite electrodes from bulk precursors for sodium-ion batteries. *Advanced Functional Materials* 29: 1900790.